

Field theory analysis of $S = 1$ antiferromagnetic bond-alternating chains in the dimer phase

Junya Tamaki

*Department of Physics, Tokyo Institute of Technology,
Oh-okayama, Meguro-ku, Tokyo 152-8551, Japan*

Masaki Oshikawa*

*Institute for Solid State Physics, University of Tokyo, Kashiwa 277-8581, Japan
(Dated: February 25, 2024)*

Dynamics of $S = 1$ antiferromagnetic bond-alternating chains in the dimer phase, in the vicinity of the critical point with the Haldane phase, is studied by a field theoretical method. This model is considered to represent the compound $\text{Ni}(\text{C}_9\text{H}_{24}\text{N}_4)(\text{NO}_2)\text{ClO}_4$ (abbreviated as NTENP). We derive a sine-Gordon (SG) field theory as a low-energy effective model of this system, starting from a Tomonaga-Luttinger liquid at the critical point. Using the exact solution of the SG theory, we give a field theoretical picture of the low-energy excitation spectrum of NTENP. Results derived from our picture are in a good agreement with results of inelastic neutron scattering experiments on NTENP and numerical calculation of the dynamical structure factor. Furthermore, on the basis of the obtained theoretical picture, we predict that the sharp peaks correspond to a single elementary excitation are absent in the Raman scattering spectrum of NTENP in contrast to the inelastic neutron scattering spectrum.

PACS numbers: 75.10.Pq, 03.70.+k, 75.40.Gb, 75.10.Jm

I. INTRODUCTION

One dimensional antiferromagnetic Heisenberg chains show various physical properties under strong quantum fluctuations. They have offered many fascinating phenomena as a stage of both theoretical and experimental studies for many years. While a uniform antiferromagnetic Heisenberg chain is gapless for half-integer spins, it has an exotic ground state with a finite gap for integer spins.¹ This gapped phase is called Haldane phase. The antiferromagnetic Heisenberg chain is not exactly solvable except for $S = 1/2$. However, the Haldane phase could be understood in terms of the solvable Affleck-Kennedy-Lieb-Tasaki model^{2,3}. Its exact ground-state can be constructed in terms of valence bonds (singlet pairs of constituent $S = 1/2$'s).

Bond-alternating antiferromagnetic Heisenberg chain defined by

$$\mathcal{H} = J \sum_j (\mathbf{S}_{2j-1} \cdot \mathbf{S}_{2j} + \alpha \mathbf{S}_{2j} \cdot \mathbf{S}_{2j+1}), \quad (1)$$

where α represents the bond alternation ratio, is an interesting generalization of the Haldane gap problem. In this model, for spin quantum number S , the system shows $2S$ successive quantum phase transitions in $0 < \alpha < \infty$ ^{4,5}. This may be understood, in the AKLT picture, as follows. In the limit of $\alpha = 0$, all the valence bonds are placed on the “odd” links between sites $2j-1, 2j$. In the opposite limit $\alpha = \infty$, all the valence bonds are placed on the “even” links between sites $2j, 2j+1$. They correspond to completely dimerized states. By changing the number of valence bonds on odd and even links, we can construct $2S+1$ AKLT-type states with varying degree of dimerization. Each of these AKLT-type states represents

the $2S+1$ gapped phases, separated by the $2S$ quantum phase transitions. Each of the transitions may be regarded as a rearrangement of valence bonds, in which one valence bond is transferred between neighboring links.

In the case of an integer spin S , $2S+1$ gapped phases can be classified into two categories: one with an even number of valence bonds on every link, and the other with an odd number of valence bonds. The latter is a (symmetry-protected) topological phase; in the presence of global $Z_2 \times Z_2$ symmetry of π -rotation about x, y and z axes, it is characterized by spontaneous breaking of a hidden $Z_2 \times Z_2$ symmetry^{6,7}, which can be detected by the string order parameter.⁸ More generally, the topological phase is also protected by either the time-reversal symmetry or the lattice inversion symmetry about a link, and is characterized by exact two-fold degeneracy of entire entanglement spectrum.^{9,10}

In this paper, we focus on the simple case of $S = 1$. Here, the $2S+1 = 3$ gapped phases consist of two dimer phases (at large and small values of α) and the $S = 1$ Haldane phase in a range of α including $\alpha = 1$. As mentioned above, being an exotic “topological phase”, the Haldane state has been studied vigorously. In contrast, the dimer phase may be regarded as a trivial phase as far as the ground-state properties are concerned, and has been relatively less studied. In fact, the system is exactly solvable in the dimer limit $\alpha = 0$, where the system is reduced to a two-body problem. However, dynamical properties, which are related to excited states, are not necessarily trivial even in the dimer phase. While quantum phases are usually classified with respect to order parameters in the ground state, they are not sufficient for elucidation of the excited states. Thus the dimer phase, although without any nontrivial order, has a possibility of exhibit-

ing a rich structure in the excitations. In addition, it would be also interesting to compare dynamical properties between the dimer phase and the Haldane phase. Therefore, in this paper, we attempt to study the dynamical properties in the $S = 1$ dimer phase, especially in the neighborhood of the quantum critical point.

Theoretical study of Haldane gap has been, without doubt, stimulated by discovery of several model materials, such as $\text{Ni}(\text{C}_2\text{H}_8\text{N}_8)_2(\text{NO}_2)\text{ClO}_4$ (abbreviated to NENP) and $\text{Ni}(\text{C}_5\text{H}_{14}\text{N}_2)_2\text{N}_3(\text{PF}_6)$ (abbreviated to NDMAP). Fortunately, materials representing the $S = 1$ bond-alternating antiferromagnetic chain (1), such as $\text{Ni}(\text{C}_9\text{H}_{24}\text{N}_4)(\text{NO}_2)\text{ClO}_4$ (abbreviated to NTENP)¹¹ and $[\text{Ni}(333\text{-tet})(\mu\text{-N}_3)_n](\text{ClO}_4)_n$ were also discovered, and the bond-alternation ratio α was identified in these materials. In the latter system, quite remarkably, α turns out to be exactly (within experimental accuracy) at the critical point separating the Haldane and dimer phases.¹² In NTENP, on the other hand, α is slightly smaller than the critical value.¹³ That is, the system belongs to the dimer phase, but in vicinity of the quantum critical point. Thus NTENP offers an ideal playground to study nontrivial dynamics in the dimer phase.

Dynamical properties of NTENP are studied experimentally by inelastic neutron scattering (INS),^{14–16} and are numerically studied by using a continued-fraction method based on the Lanczos algorithm¹⁷. However, in order to better understand the dynamics in NTENP and also in related materials in a unified way, it would be desirable to develop a coherent theoretical picture. In this paper, we present a field theoretical approach to the problem, which we hope would serve the purpose.

At a quantum critical point, physical quantities are often constrained by the conformal invariance, and the system is described by a conformal field theory (CFT). Near the critical point, the system could be understood by a CFT with a small (but relevant) perturbation. In this paper, we follow this strategy, making use of the feature of NTENP that the bond-alternating ratio is in the vicinity of the critical point. Based on the obtained effective theory, we elucidate the dynamical properties of NTENP and discuss preceding experimental and numerical results. Furthermore, we make predictions on Raman Scattering experiment which has not yet been carried out.

II. MODEL AND METHOD

In fact, NTENP has a sizable spin anisotropy; it is better described, instead of eq. (1), by the following Hamiltonian¹³

$$\mathcal{H} = J \sum_j (\mathbf{S}_{2j-1} \cdot \mathbf{S}_{2j} + \alpha \mathbf{S}_{2j} \cdot \mathbf{S}_{2j+1}) + D \sum_j (S_j^z)^2, \quad (2)$$

where $J > 0$, α and D represent bond alternation and uniaxial anisotropy, respectively. For NTENP, these parameters are $D \sim 0.25J$ and $\alpha \sim 0.45$. The spin

anisotropy axis (which is determined by the chain axis) is taken to be z -direction. In this paper, we ignore the in-plane anisotropy $E \sum_j (S_j^x)^2 - (S_j^y)^2$ and the exchange anisotropy, which are expected to be smaller than D in NTENP. The lattice constant between neighboring two spins is set to unity.

The critical point α_c , where energy gap is closed, is about 0.6 at $D = 0$. It is a function of D which is numerically evaluated in Ref. 18. According to them, α_c is almost constant for $0 < D \lesssim 0.3J$. In NTENP, $D \sim 0.25J$ and thus we can assume that $\alpha_c \sim 0.6$. The actual bond-alternating ratio of NTENP is $\alpha \sim 0.45 < \alpha_c$, and the system is certainly in the dimer phase. However, it can be still regarded as a vicinity of the quantum critical point.

At the critical point $\alpha = \alpha_c$, the system is mapped to a TL liquid,¹⁹ in the low-energy limit.¹³ It is nothing but the theory of free boson field ϕ with the Lagrangian density,

$$\mathcal{L} = \frac{1}{2}(\partial_\mu \phi)^2. \quad (3)$$

Let R be the compactification radius of boson field,

$$\phi(x, t) + 2\pi R \sim \phi(x, t). \quad (4)$$

The compactification radius determines critical exponents of the TL liquid. This may be understood as a consequence of “quantization” of vertex operators required by the compactification. For example, the vertex operators $\cos(\gamma\phi)$ must have the coefficient $\gamma = n/R$ with an integer n , in order to be single-valued under the compactification (4). The scaling dimension of the vertex operator $\cos(n\phi/R)$ is known¹⁹ as

$$x_n = \frac{n^2}{4\pi R^2}. \quad (5)$$

The operator is relevant (irrelevant) in the Renormalization-Group (RG) sense, if the scaling dimension is smaller (greater) than 2. Thus, among the vertex operators of the above form, $n = 1$ is the most relevant. As we will discuss later, in the present application R is somewhat smaller than the $\text{SU}(2)$ symmetric value $1/\sqrt{2\pi}$, implying $n = 1$ is the only relevant operator in the family $\cos(n\phi/R)$.

When $\alpha \neq \alpha_c$, the system acquires a gap and it is no longer described by the TL liquid (3). However, if $|\alpha - \alpha_c|$ is small, as it is the case in NTENP, the low-energy effective theory would be given by the TL liquid with a perturbation. We postulate that the leading perturbation is the most relevant operator permitted under the symmetry of the Hamiltonian (2): $\cos(\phi/R)$. Hence the low-energy effective theory for small $|\alpha - \alpha_c|$ should be following sine-Gordon (SG) field theory,

$$\mathcal{L} = \frac{1}{2}(\partial_\mu \phi)^2 + C \cos\left(\frac{\phi}{R}\right), \quad (6)$$

where C is the constant that is proportional to $\alpha - \alpha_c$ and R is the compactification radius of boson field at the

critical point. When $\alpha = \alpha_c$, C equals zero and Eq. (6) is reduced to Eq. (3). It should be noted that we use R at the critical point α_c in this construction (6) for $\alpha \neq \alpha_c$. The compactification radius R is well defined only at the critical point and the precise determination of R is subtle for $\alpha \neq \alpha_c$. Nevertheless, R obtained at $\alpha = \alpha_c$ should be a reasonable approximation as long as $|\alpha - \alpha_c|$ is small. We also note that R at the critical point α_c is a function of D .

The SG field theory is integrable and its exact solution is known.^{20,21} In this study, we analyze the low-energy spectrum of NTENP using the exact solution of the SG field theory, where the original spin Hamiltonian is mapped. We thus refer to this exact solution in the next section.

III. EXACT SOLUTION OF THE SINE-GORDON FIELD THEORY

The SG field theory has the Lorentz invariance, hence the energy of the elementary excitations obey the relativistic dispersion relation

$$\epsilon = \sqrt{k^2 v_s^2 + m^2}. \quad (7)$$

Here, v_s is the spin-wave velocity which plays the role of the speed of light, k is the momentum, and m is the mass of the excitation (in the unit of energy), which represents the lowest creation energy of each elementary excitations.

The elementary excitations of the SG field theory (6) consist of a soliton, an antisoliton and several breathers. The soliton and the antisoliton have the same mass M_S . Breathers are bound states of a soliton and an antisoliton. The exact solution^{20,21} of the SG field theory implies the number of different kinds of breathers as $[1/\xi]$, where

$$\frac{1}{\xi} = 8\pi R^2 - 1, \quad (8)$$

and $[x]$ denotes the integer part of x . Remarkably, the exact mass ratio was also derived as

$$\frac{M_n}{M_S} = 2 \sin\left(\frac{n\pi\xi}{2}\right) \quad (n < 1/\xi), \quad (9)$$

where M_n and M_S are respectively the n -th breather mass and the soliton mass. Here we note that the breather mass M_n does not exceed twice the soliton mass $2M_S$. Physically, this can be interpreted as follows. If the mass of a breather were larger than $2M_S$, the breather would decay into free soliton and antisoliton, and would not constitute a stable elementary excitation. It should be emphasized that the mass ratio (9) and the number of different breathers depend only on the boson field compactification radius R , which is a function of D .

The above picture of elementary excitations implies the spectrum of the excited states schematically described in Fig. 1. Each elementary excitation obeys the relativistic dispersion (7) with a species-dependent mass m and the

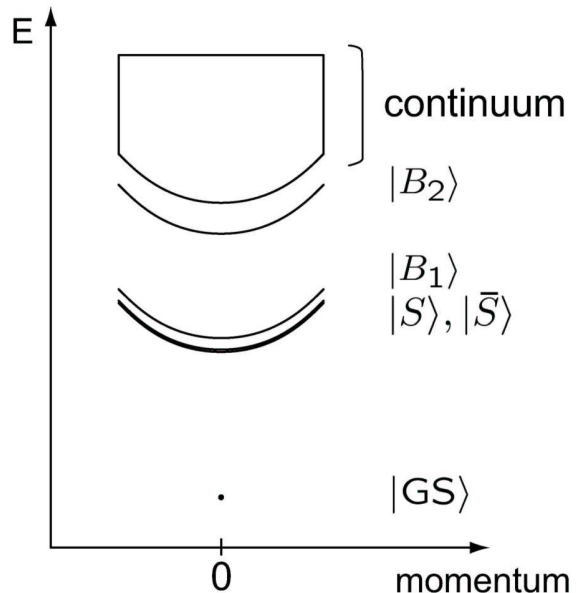


FIG. 1. Schematic view of the excitation spectrum of the SG field theory. $|GS\rangle$, $|S\rangle$, $|\bar{S}\rangle$, $|B_1\rangle$ and $|B_2\rangle$ represent the ground state, the soliton state, the antisoliton state, the first breather state and the second breather state, respectively. The soliton level and the antisoliton level is degenerated. The number of different breathers is $[1/\xi]$, where $[x]$ denotes the integer part of x and $1/\xi = \frac{2}{\pi R^2} - 1$. In this schematic view, the case that the theory has two breathers is represented. Owing to the Lorentz invariance of the theory, the excitation energies obey the relativistic dispersion relation (7).

common spin-wave velocity v_s . Above the energy $2M_S$, there is a continuum of excited states, corresponding to scattering states of two or more elementary excitations.

The elementary excitations of NTENP is understood as the corresponding elementary excitations of the SG field theory. The boson field compactification radius R of NTENP determines the mass ratio between a soliton and breathers and the number of different breathers correspond to NTENP.

In passing, we note that, for an isotropic system, the $SU(2)$ symmetry requires $R = 1/\sqrt{2\pi}$. The exact solution of the SG theory implies that there are two breathers, and the mass of the 1st breather is degenerate with soliton/antisoliton, forming a $SU(2)$ triplet. Furthermore, the mass of the second breather is $\sqrt{3}$ times that of the triplet. However, this does not quite agree with the numerical results. This is due to the marginal perturbation to the SG theory, which generally exists in the $SU(2)$ symmetric system. Only with an appropriate strength of next-nearest neighbor interaction, the marginal operator can be eliminated and the above prediction of the SG theory is realized^{22,23}. In this paper, however, we consider a system with a substantial anisotropy, where the marginal operator is absent. Thus the simple SG theory (6) is expected to be a good low-energy effective theory of the system.

IV. STRUCTURE OF ELEMENTARY EXCITATIONS

A. Mass ratio among the elementary excitations

We are now in a position to apply the relation (9) to the system of NTENP. Here we note again that the critical point α_c and the compactification radius R at this point are a function of the uniaxial anisotropy D . At $D = 0$, R is determined as $2\pi R^2 = 1$ by the $SU(2)$ symmetry of the system. The variation of R at several values of D is already studied numerically by using CFT and the level spectroscopy method, by Chen et al.¹⁸ The parameter K , δ and D in Ref. 18 correspond to $1/(2\pi R^2)$, $(1 - \alpha)/(1 + \alpha)$ and $2D/(1 + \alpha)$ respectively, in the notation of the present paper. Thus, for NTENP with $D \sim 0.25J$, we find $1/(2\pi R^2) \sim 1.7$ that implies $1/\xi \sim 1.2$. It follows that this effective SG field theory for NTENP has the first breather only. The breather/soliton mass ratio is

$$b = \frac{M_1}{M_S} = 1.93. \quad (10)$$

Accordingly, the energy spectrum of NTENP based on the SG field theory picture appears to be the following: the lowest excited state is a degenerate doublet corresponds to the soliton and the antisoliton, the next lowest excited state is a single mode corresponds to the breather, and an excitation continuum starts from the energy twice the soliton mass. This spectrum is schematically described in Fig. 4.

B. Dynamical structure factor

The dynamical structure factor (DSF) is defined as the Fourier transform of the correlation function. It is an important quantity, as the differential cross section in an INS is proportional to the DSF. The μ ($= x, y, z$) component of the DSF at zero temperature is

$$\begin{aligned} \mathcal{S}^{\mu\mu}(q, \omega) &= \int_{-\infty}^{\infty} dt \sum_{j,k} \langle \psi_0 | S_j^\mu(t) S_k^\mu(0) | \psi_0 \rangle e^{i\omega t - iq(j-k)} \\ &= \sum_n \delta(\omega - (E_n - E_0)) |\langle \psi_n | S_q^\mu | \psi_0 \rangle|^2, \end{aligned} \quad (11)$$

where $|\psi_0\rangle$ and $|\psi_n\rangle$ are the ground state and the excited state of Hamiltonian (2) with the eigenvalue E_0 and E_n , respectively, and $S_q^\mu = \frac{1}{\sqrt{2N}} \sum_{j=1}^{2N} S_j^\mu e^{-iqj}$, where $2N$ is the total number of spins. Here it should be noted that, in the systems with a bond alternation such as NTENP, the width of the Brillouin zone is reduced to half of that of the uniform chain. Namely, the conserved crystal momentum can be defined as

$$\tilde{q} = q \pmod{\pi}, \quad (12)$$

which is defined on the reduced Brillouin zone

$$-\pi/2 \leq \tilde{q} < \pi/2 \quad (13)$$

In particular, $q = 0$ and $q = \pi$ are both identified with the center of the reduced Brillouin zone $\tilde{q} = 0$. However, it should be noted that, the DSF is *not* equivalent for q and $q + \pi$. This could be easily understood by considering the limit of zero dimerization, where q and $q + \pi$ are certainly distinguishable. The operator S_q^μ and $S_{q+\pi}^\mu$ are different operators and thus give different DSFs. In the presence of dimerization, they are governed by the same selection rule. The matrix elements, however, are generally different.

The summation in Eq. (11) is taken over all intermediate states, but many of the matrix elements vanish due to selection rules. While excited states $|\psi_n\rangle$ contain one or more elementary excitations, only the states which have non-vanishing overlap with $S_q^\mu |\psi_0\rangle$ contribute to the DSF. Thus, in order to evaluate each component of the DSF, it is important to know what kind of elementary excitations are created by applying S_q^μ on the ground state $|\psi_0\rangle$. For example, if $S_q^\mu |\psi_0\rangle$ contains a single soliton state, there must be a contribution proportional to $\delta(\omega - \sqrt{\tilde{q}^2 + M_S^2})$, to $\mathcal{S}^{\mu\mu}(q, \omega)$.

C. Dimer limit

In order to clarify which elementary excitation is created by application of each spin operator, we need to know the correspondence between the operators in the SG field theory and those in the original spin system. In principle, this would follow from a microscopic derivation of the effective SG field theory from the spin model (2). However, the microscopic derivation is rather complicated and the correspondence cannot be easily established. A possible derivation starts from the bosonization of two $S = 1/2$ chains and then introduces a strong ferromagnetic coupling between them, to form a $S = 1$ chain effectively²⁴. Instead of pursuing this direction, we shall develop a simple ansatz for the correspondence, based on the dimer limit $\alpha = 0$.

In the dimer limit, the problem is reduced to a two-spin problem, and thus can be exactly solved. Two $S = 1$'s coupled with the Heisenberg antiferromagnetic exchange, $\mathcal{H} = J\mathbf{S}_1 \cdot \mathbf{S}_2$ has the singlet groundstate with energy $-2J$, triplet excited states with energy $-J$, quintet excited states with energy $+J$. Now let us introduce the uniaxial anisotropy D to the dimer, and consider the Hamiltonian

$$\mathcal{H} = J\mathbf{S}_1 \cdot \mathbf{S}_2 + D((S_1^z)^2 + (S_2^z)^2). \quad (14)$$

The singlet groundstate is perturbed by the anisotropy, and given by

$$|s\rangle = C_s \left(|\uparrow\downarrow\rangle + |\downarrow\uparrow\rangle + \frac{4}{A - \sqrt{A^2 + 8}} |00\rangle \right), \quad (15)$$

with the groundstate energy

$$\frac{A - \sqrt{A^2 + 8}}{2} J, \quad (16)$$

where $A = 2D - 1$ and C_s is the normalization constant.

The uniaxial anisotropy splits the triplet and quintet excited states. Each state can be labelled by the total magnetization $S^z = S_1^z + S_2^z$, which is still a good quantum number. Since the uniaxial anisotropy does not break the π -rotation symmetry under rotation about x -axis. Thus, the triplet states are split into a singlet with $S^z = 0$, which is denoted by $|t^0\rangle$, and a doublet $|t^\pm\rangle$ with $S^z = \pm 1$. The doublet states are given by

$$|t^+\rangle = \frac{1}{\sqrt{2}}(|\uparrow 0\rangle - |0 \uparrow\rangle), \quad (17)$$

$$|t^-\rangle = \frac{1}{\sqrt{2}}(|\downarrow 0\rangle - |0 \downarrow\rangle), \quad (18)$$

with the energy $D - J$, while the singlet is given by

$$|t^0\rangle = \frac{1}{\sqrt{2}}(|\uparrow\downarrow\rangle - |\downarrow\uparrow\rangle), \quad (19)$$

with the energy $2D - J$. For $D > 0$, which is the case for NTENP, the doublet states $|t^\pm\rangle$ are lower in energy than the singlet $|t^0\rangle$.

In a similar way, the quintet states are split into a singlet with $S^z = 0$ and two doublets with $S^z = \pm 1$ and $S^z = \pm 2$. However, as we will argue below, once we move away from the dimer limit, they decay into excitations corresponding to $|t^{0,\pm}\rangle$. Thus, for the purpose of classification of elementary excitations, it is sufficient to consider the (split) triplet $|t^{0,\pm}\rangle$.

Given these states in single dimers, the states in the entire system is given as follows: The ground state is the state that all dimers form $|s\rangle$. The lowest excited state is the state that $|t^+\rangle$ or $|t^-\rangle$ is excited in one of the dimers, while the other dimers remain in $|s\rangle$. Similarly in the next lowest excited state, $|t^0\rangle$ is excited in one of the dimers and the other dimers form $|s\rangle$. Here, we denote these states $|0\rangle$, $|\text{one } t^+\rangle$, $|\text{one } t^-\rangle$, and $|\text{one } t^0\rangle$, respectively. In fact, in a system which consists of N dimers ($2N$ sites), there are N degenerate states for each class of $|\text{one } t^\zeta\rangle$, where $\zeta = 0, \pm$, corresponding to the location of the excited dimer. Let us define $|\text{one } t^\zeta, j\rangle$, where $\zeta = 0, \pm$, as the state with the j -th dimer (of sites $2j - 1$ and $2j$) as the only excited dimer. We can also define their Fourier transform

$$|\text{one } t^\zeta, \tilde{q}\rangle \equiv \frac{1}{\sqrt{N}} \sum_j e^{i2j\tilde{q}} |\text{one } t^\zeta, j\rangle, \quad (20)$$

where $\zeta = 0, \pm$, labeled by the crystal momentum \tilde{q} defined in the reduced Brillouin zone (13).

In this paper, we are primarily interested in the DSF around the antiferromagnetic wavevector, $q \sim \pi$. Here, the matrix elements of spin operators among these states are found to be:

$$\begin{aligned} \langle \text{one } t^+, \tilde{q} | S_q^+ | 0 \rangle &\neq 0, \\ \langle \text{one } t^-, \tilde{q} | S_q^- | 0 \rangle &\neq 0, \\ \langle \text{one } t^0, \tilde{q} | S_q^z | 0 \rangle &\neq 0, \end{aligned} \quad (21)$$

generically if $\tilde{q} \equiv q \pmod{\pi}$, and

the other matrix elements of S_q^μ
between $|0\rangle$ and $|\text{one } t^\pm\rangle$, or $|\text{one } t^0\rangle = 0$.

Now let us consider increasing α from zero. With a nonzero α , an excited state in a single dimer can “hop” to the neighboring sites, giving rise to a dispersion. It should be noted that, in the dimerized limit, the momentum basis (20) as well as the localized basis $|\text{one } t^\zeta, j\rangle$, represents N degenerate excited states. However, when the interdimer interaction is introduced with $\alpha > 0$, momentum basis (20), but not the localized basis gives a set of approximate eigenstates if α is sufficiently small. Now the energy of the excited state $|\text{one } t^\zeta, \tilde{q}\rangle$ depends on the momentum \tilde{q} ; the dependence is nothing but the dispersion relation. Since the structure of the triplet split into the doublet and the singlet by the anisotropy is very similar between the single dimer and the SG field theory, it would be natural to assume that the structure of the excitation does not qualitatively change in $0 \leq \alpha < \alpha_c$. Under this assumption, the states in the dimer limit $\alpha = 0$, $|0\rangle$, $|\text{one } t^+\rangle$, $|\text{one } t^-\rangle$ and $|\text{one } t^0\rangle$ are considered to be smoothly connected to, at $\alpha \sim \alpha_c$, the ground state $|\text{GS}\rangle$, and the single soliton state $|S, \tilde{q}\rangle$, the single antisoliton state $|\bar{S}, \tilde{q}\rangle$, the single breather state $|B_1, \tilde{q}\rangle$, each with the momentum \tilde{q} . If this is the case, the following selection rules should hold:

$$\begin{aligned} \langle S, \tilde{q} | S_q^+ | \text{GS} \rangle &\neq 0, \\ \langle \bar{S}, \tilde{q} | S_q^- | \text{GS} \rangle &\neq 0, \\ \langle B_1, \tilde{q} | S_q^z | \text{GS} \rangle &\neq 0, \end{aligned} \quad (22)$$

generically if $\tilde{q} \equiv q \pmod{\pi}$, and

the other matrix elements of S_q^μ
between $|\text{GS}\rangle$ and $|S, \tilde{q}\rangle$, $|\bar{S}, \tilde{q}\rangle$, or $|B_1, \tilde{q}\rangle = 0$

Assuming this, S_q^+ , S_q^- and S_q^z respectively act as the creation operators of the soliton, the antisoliton and the breather. Thus the soliton and the antisoliton contribute to the x, y components of the DSF and the breather does to the z component.

The assumption above is natural because we are interested in a system in the dimer phase, and there is no phase transition between the dimer limit $\alpha = 0$. However, properties of excited states are not necessarily the same, even if they are in the same phase and the ground-states are adiabatically connected. We confirmed the validity of our assumption and that the matrix elements in Eq. (22) does not vanish, by the numerical exact diagonalization calculation using the Lanczos method. We show our numerical results in Fig. 2 and Fig. 3. In what follows, we direct our attention to the states with $\tilde{q} = 0$ which correspond to the bottom of the each branch in the energy spectrum, in order to compare with the preceding results.^{14,15,17} As we will clarify later, it suffices to obtain the matrix element of the local spin operator S_j^α between the groundstate and the excited states.

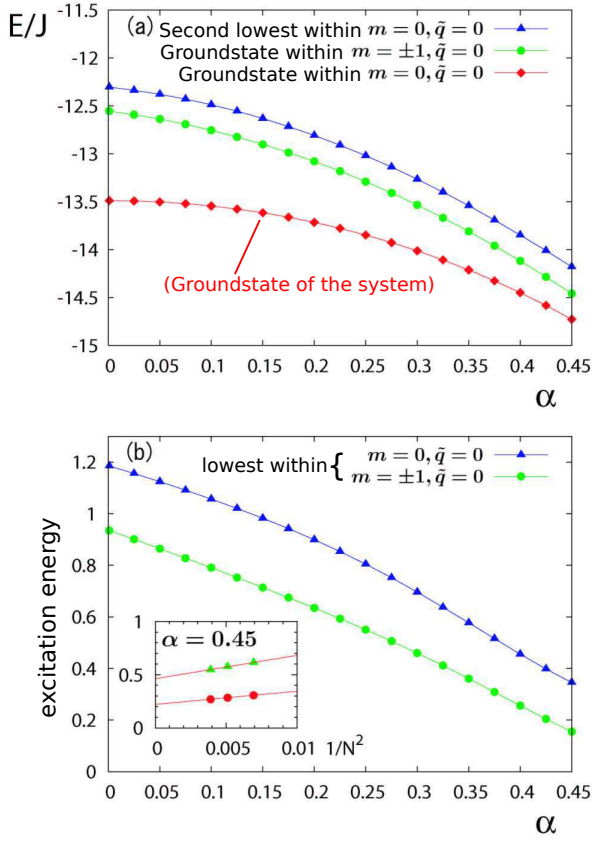


FIG. 2. (a) The α -dependence of the energy of the ground state and the lowest excited state in subspaces that the total magnetization $m = \sum_j S_j^z$ is $\pm 1, 0$ and the momentum $\tilde{q} = 0$. ($N = 16$) The case that $\alpha = 0.45$ corresponds to NTENP. (b) The excitation energies extrapolated to $N \rightarrow \infty$. Inset: Extrapolation of the excitation energies at $\alpha = 0.45$ to $N \rightarrow \infty$.

Fig. 2 (a) shows the energy of the ground state and the lowest excited state in subspaces that the total magnetization $m = \sum_j S_j^z$ is $\pm 1, 0$ and the momentum $\tilde{q} = 0$. This figure is obtained by the exact diagonalization of the 16 site spin system. Fig. 2 (b) shows the excitation energies extrapolated from the calculated values in the 12, 14 and 16 site spin systems to the infinite size. These results show that the energy of the elementary excitations changes adiabatically under the variation of α from 0 to 0.45 ($\sim \alpha_c$), which is the value of NTENP. Thus our assumption that the excitation structure evolves smoothly under the variation of α , is confirmed. In what follows, we represent the states at α that are adiabatically connected from $|\phi\rangle$ at $\alpha = 0$, as $|\phi\rangle_\alpha$. The states $|\text{one } t^+\rangle_{\alpha \sim \alpha_c}$, $|\text{one } t^-\rangle_{\alpha \sim \alpha_c}$ and $|\text{one } t^z\rangle_{\alpha \sim \alpha_c}$ correspond to the soliton $|S\rangle$, the antisoliton $|\bar{S}\rangle$ and the breather $|B_1\rangle$, respectively. When α is finite, the elementary excitations have a dispersion. Therefore we label them also with the momentum \tilde{q} .

Fig. 3 shows the absolute value of the matrix ele-

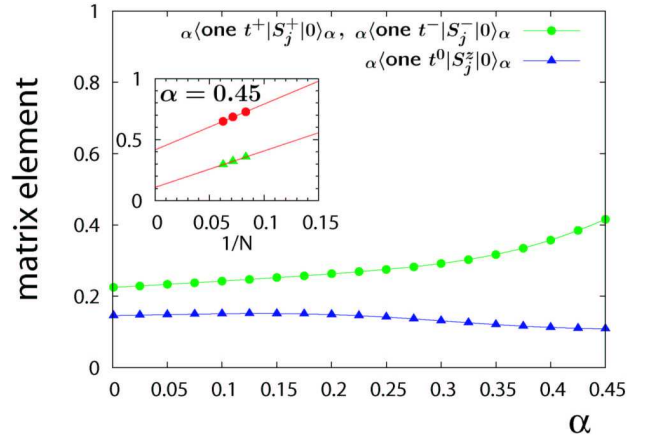


FIG. 3. The α -dependence of the absolute value of the matrix elements $\alpha \langle \text{one } t^+, \tilde{q} = 0 | S_j^+ | 0 \rangle_\alpha$, $\alpha \langle \text{one } t^-, \tilde{q} = 0 | S_j^- | 0 \rangle_\alpha$ and $\alpha \langle \text{one } t^0, \tilde{q} = 0 | S_j^z | 0 \rangle_\alpha$. ($N = 16$) They correspond to $\langle S | S_j^+ | \text{GS} \rangle$, $\langle \bar{S} | S_j^- | \text{GS} \rangle$ and $\langle B_1 | S_j^z | \text{GS} \rangle$ in the vicinity of the critical point $\alpha = \alpha_c$, respectively. Inset: Extrapolation of the matrix elements at $\alpha = 0.45$ to $N \rightarrow \infty$.

ments $\alpha \langle \text{one } t^+, \tilde{q} = 0 | S_j^+ | 0 \rangle_\alpha$, $\alpha \langle \text{one } t^-, \tilde{q} = 0 | S_j^- | 0 \rangle_\alpha$ and $\alpha \langle \text{one } t^0, \tilde{q} = 0 | S_j^z | 0 \rangle_\alpha$ in the variation of α . This figure is also obtained by the 16 site spin system exact diagonalization. From these calculated values, the matrix elements of S_q^μ corresponding to them are evaluated as follows: As we will discuss later in Sec. VI, the ground state $|0\rangle$ is link-parity even, and the states $|\text{one } t^+, \tilde{q} = 0\rangle_\alpha$, $|\text{one } t^-, \tilde{q} = 0\rangle_\alpha$ and $|\text{one } t^z, \tilde{q} = 0\rangle_\alpha$ are link-parity odd:

$$P_l |0\rangle_\alpha = |0\rangle_\alpha, \\ P_l |\text{one } t^\zeta, \tilde{q} = 0\rangle_\alpha = -|\text{one } t^\zeta, \tilde{q} = 0\rangle_\alpha,$$

where $\zeta = 0, \pm$, and the link parity operator P_l represents a reflection with respect to a link. It satisfies $P_l^2 = I$, where I is the identity operator. From these properties, it follows that

$$\begin{aligned} \alpha \langle \text{one } t^\zeta, \tilde{q} = 0 | S_{j+1}^+ | 0 \rangle_\alpha &= \alpha \langle \text{one } t^\zeta, \tilde{q} = 0 | P_l S_j^+ P_l | 0 \rangle_\alpha \\ &= -\alpha \langle \text{one } t^\zeta, \tilde{q} = 0 | S_j^+ | 0 \rangle_\alpha, \end{aligned} \quad (23)$$

where $\zeta = 0, \pm$. Accordingly, $\alpha \langle \text{one } t^\zeta, \tilde{q} = 0 | S_{q=\pi}^+ | 0 \rangle_\alpha$ does not vanish, while $\alpha \langle \text{one } t^\zeta, \tilde{q} = 0 | S_{q=0}^+ | 0 \rangle_\alpha = 0$. The adiabatic continuity of the excited states then implies the same selection rule for the single soliton state $|S, \tilde{q} = 0\rangle$, single antisoliton state $|\bar{S}, \tilde{q} = 0\rangle$, and single breather state $|B_1, \tilde{q} = 0\rangle$. Thus we have confirmed the validity of our ansatz.

D. Excitation structure of NTENP based on the SG field theory

Combining the results in Secs. IV A and IV B, we obtain the following picture: NTENP has three elementary

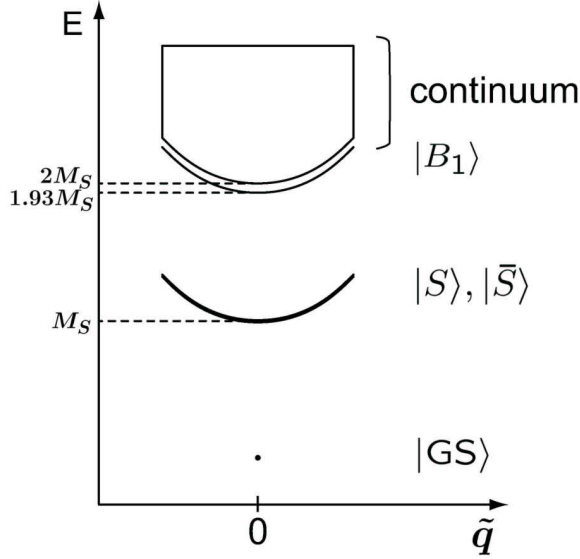


FIG. 4. Schematic view of the excitation spectrum of NTENP based on the SG field theory. The doubly degenerated isolated mode correspond to the soliton and the antisoliton is present and its lowest creation energy is M_S . The system has only the first breather and its lowest creation energy is $1.93M_S$. The excitation continuum starts from the $2M_S$ at the momentum $\tilde{q} = 0$.

excitations that correspond to the soliton, the antisoliton and the first breather in the SG theory. For these elementary excitations, the soliton mass and the antisoliton mass are degenerate, and the first breather mass is 1.93 times the soliton mass. (The mass degeneracy of soliton/antisoliton is a common nature of the SG field theories, that is, irrespective of the value of radius R . On the other hand, the breather mass ratio depends on the value of the radius R . For NTENP, $1/(2\pi R^2) \sim 1.7$.) Thus, it is concluded that the doubly degenerated isolated mode is at M_S and the single isolated mode is at $1.93M_S$ in the energy spectrum of NTENP. The excitation continuum starts from $2M_S$. This is schematically described in Fig. 4.

The soliton, the antisoliton and the breather are respectively created by operating S_q^+ , S_q^- and S_q^z on the ground state. Conversely, when each spin operator creates a single elementary excitation, its species is uniquely determined as soliton, antisoliton, and breather. Hence the single-particle peak due to the soliton/antisoliton contribute only to \mathcal{S}^{xx} and \mathcal{S}^{yy} , and that due to the breather does to only \mathcal{S}^{zz} . The intensity ratio between the lowest excited states in \mathcal{S}^{xx} and \mathcal{S}^{zz} are evaluated from the result in Fig. 3. Since the bottom of each elementary excitation branch in the energy spectrum $\tilde{q} = 0$ corresponds to $q = 0$ and $q = \pi$, the intensity from the lowest excited state in $\mathcal{S}^{\mu\mu}$ is the sum of $\mathcal{S}^{\mu\mu}(0, \omega)$ and $\mathcal{S}^{\mu\mu}(\pi, \omega)$ (where ω is the energy transfer of the lowest excited state). However, the matrix elements of $S_{q=0}^\mu$ vanishes due to the relation (23) for each elementary exci-

tations, then only those of $S_{q=\pi}^\mu$ contribute. For example, the contribution of the soliton with $\tilde{q} = 0$ occurs in $\mathcal{S}^{xx}(\pi, \omega_S)$. Taking these into consideration, the intensity ratio are evaluated by

$$\frac{|\langle B_1, \tilde{q} = 0 | S_{q=\pi}^z | \text{GS} \rangle|^2}{\frac{1}{4} |\langle S, \tilde{q} = 0 | S_{q=\pi}^+ | \text{GS} \rangle|^2 + \frac{1}{4} |\langle \bar{S}, \tilde{q} = 0 | S_{q=\pi}^- | \text{GS} \rangle|^2} \sim 0.22. \quad (24)$$

Here, we use the calculated values $_{0.45} \langle \text{one } t^+, \tilde{q} = 0 | S_{q=\pi}^+ | 0 \rangle_{0.45}$, $_{0.45} \langle \text{one } t^-, \tilde{q} = 0 | S_{q=\pi}^- | 0 \rangle_{0.45}$ and $_{0.45} \langle \text{one } t^z, \tilde{q} = 0 | S_{q=\pi}^z | 0 \rangle_{0.45}$ in Fig. 3 for the soliton, the antisoliton and the breather, respectively.

V. COMPARISON WITH PRECEDING RESULTS

According to Refs. 14 and 15, two main peaks are present in the INS spectrum of NTENP. The first peak occurs from the fluctuation of spin x, y components and the second from that of z component. In an inelastic scan at the center of the Brillouin zone, the energy ratio between the peak from spin x, y component and that from z component is about $1.91/1.07 \sim 1.79$, and the intensity of the second peak is about 0.2 times that of the first peak. Furthermore, the DSF in the model (2) under a transverse magnetic field H is numerically studied using the continued-fraction method¹⁷. Their result at $H = 0$ can be compared with the present study. The ratio between the energies correspond to the first peak in $\mathcal{S}^{xx}(\pi, \omega)$ and $\mathcal{S}^{zz}(\pi, \omega)$ is ~ 1.91 and the intensity of the first peak of $\mathcal{S}^{zz}(\pi, \omega)$ is about 0.22 times that of $\mathcal{S}^{xx}(\pi, \omega)$. We also note that, the ratio of the lowest gap to $m = \pm 1$ and $m = 0$ excitations in our exact diagonalization study, shown in Fig. 2, is consistent with the predicted mass ratio 1.93. This gives an additional support to our field-theory analysis.

The lowest-energy peak in the INS spectrum in Refs. 14 and 15, which corresponds¹⁷ to the lowest excited state in $\mathcal{S}^{xx}(\pi, \omega)$, is the contribution of the soliton/antisoliton in our picture. Likewise, the second peak in the INS spectrum, which corresponds to the lowest excited state in $\mathcal{S}^{zz}(\pi, \omega)$, is the contribution of the breather. Our results that the mass ratio between soliton and breather $M_B/M_S \sim 1.93$ and that the creation operator of soliton, antisoliton and breather is respectively S_q^+ , S_q^- and S_q^z , agree very well with these results. Our result (24) on the intensity ratio also shows a good agreement. Not only the peak positions but also the polarization of the DSF is consistent. Our field-theory approach thus provides a coherent theoretical picture describing the preceding experimental and numerical results, at least at zero magnetic field. A slight disagreement with experiments may be attributed to the following factors. First, we neglected the in-plane anisotropy E , which must be present in NTENP with a triclinic crystal structure. Furthermore, the low-energy asymptotic description based

on the SG field theory is not exact for NTENP due to its finite energy gap.

More recently, ESR study of NTENP was reported in Ref. 25. We will make a brief comment on ESR in Sec. VII.

VI. RAMAN SCATTERING IN NTENP

As a new application of the present approach, in this section, we discuss the Raman scattering (RS) spectrum of NTENP and predict its peak positions. Following our discussion in Sec. IV B, we first identify the non-vanishing matrix elements in the dimer limit $\alpha = 0$, and then extend the results to $\alpha \neq 0$ using the continuity of the excitation structure from $\alpha = 0$ to $\alpha \lesssim \alpha_c$.

According to the theory of exchange-scattering in magnetic compounds, the spectral function $I(\omega)$ for the scattered light at zero temperature is given by ²⁶

$$I(\omega) = \sum_n \delta(\omega - (E_n - E_0)) |\langle \psi_n | \mathcal{H}_R | \psi_0 \rangle|^2, \quad (25)$$

where $|\psi_0\rangle$ and $|\psi_n\rangle$ are the ground state and the excited state of the Hamiltonian (2), whose energy eigenvalues are E_0 and E_n , and \mathcal{H}_R is the effective interaction for the exchange-scattering of light,

$$\mathcal{H}_R = \sum_i (\mathbf{e}_i \cdot \mathbf{d}_{i,i+1}) (\mathbf{e}_s \cdot \mathbf{d}_{i,i+1}) (\mathbf{S}_i \cdot \mathbf{S}_{i+1}), \quad (26)$$

for the present one dimensional system (2). Here, \mathbf{e}_i , \mathbf{e}_s are unit polarization vectors of incident and scattered light, and $\mathbf{d}_{i,i+1}$ is a unit vector connecting the spin sites i and $i+1$. In Eq. (26), $\mathbf{d}_{i,i+1}$ is constant in the present system (2); once the experimental apparatus is set up, \mathbf{e}_i and \mathbf{e}_s are fixed. (For a recent discussion of related problems, see Ref. 27.) Thus, we just need to know matrix elements of the operator $\sum_i \mathbf{S}_i \cdot \mathbf{S}_{i+1}$ in order to calculate RS spectrum. This effective Raman Hamiltonian (26), taking the form of an inner products of spin operators, possesses several symmetries. Consequently, there are following conserved quantities: the total magnetization $m = \sum_j S_j^z$, the momentum and the link parity of the states. Link parity transformation is a reflection with respect to a link. In the systems with bond alternation such as NTENP, the link parity is conserved but the site parity (reflection with respect to a site) is not conserved. The link parity operator P_l satisfies $P_l^2 = I$, where I is the identity operator. As mentioned above, the selection rule for RS is quite different from that for INS represented in Eq. (11). This difference leads to distinct peak positions between the INS and the RS spectrum of NTENP.

In what follows, we discuss the overlaps between $|\psi_n\rangle$ and $|\psi_0\rangle$ to detect the excited states that contribute to the RS spectrum. For this purpose, here we collect the conserved quantities in the present system (2) again: the

total magnetization $m = \sum_j S_j^z$, the momentum \tilde{q} associated with the invariance under the translation by two sites, and the link parity.

First we analyze the $\alpha = 0$ case. The ground state $|0\rangle$ is the eigenstate of m with the eigenvalue 0, while the lowest excited states $|\text{one } t^+\rangle$ and $|\text{one } t^-\rangle$ are that with the eigenvalue 1 and -1 , respectively. Since \mathcal{H}_R conserves the total magnetization m , these excited states do not have overlap with $\mathcal{H}_R|0\rangle$, and do not contribute to the RS spectrum. Thus in what follows, we only discuss the subspace with $m = 0$ in order to detect the states having non-vanishing overlap with $\mathcal{H}_R|0\rangle$. The three low-energy excited states in this subspace, applied the same notation as the preceding one, are $|\text{one } t^0\rangle$, $|\text{one } t^+\rangle$, $|\text{one } t^-\rangle$, and $|\text{two } t^0\rangle$, from the lowest in energy, in the dimer limit $\alpha = 0$. They correspond to the single breather state, the scattering state of a soliton and an antisoliton, and the scattering state of two breathers, respectively at $\alpha \sim \alpha_c$.

The link parity of the ground state $|0\rangle$ and these states are calculated as follows: For a given state $|\phi\rangle$, we denote its mapping by the link parity as $|\bar{\phi}\rangle = P_l|\phi\rangle$. As a preparation, we first discuss the link parity of the states in a single dimer. The state $|s\rangle$ is link-parity even:

$$\begin{aligned} |\bar{s}\rangle &= P_l|s\rangle = C_s P_l (|\uparrow\downarrow\rangle + |\downarrow\uparrow\rangle) + \frac{4}{A - \sqrt{A^2 + 8}} |00\rangle \\ &= C_s (|\downarrow\uparrow\rangle + |\uparrow\downarrow\rangle) + \frac{4}{A - \sqrt{A^2 + 8}} |00\rangle \\ &= |s\rangle, \end{aligned} \quad (27)$$

where $A = 2D - 1$ and C_s is the normalization constant. In a similar calculation, we find that the states $|t^0\rangle$, $|t^+\rangle$, and $|t^-\rangle$ are link-parity odd:

$$|\bar{t}^0\rangle = P_l|t^0\rangle = -|t^0\rangle, \quad (28)$$

$$|\bar{t}^+\rangle = P_l|t^+\rangle = -|t^+\rangle, \quad (29)$$

$$|\bar{t}^-\rangle = P_l|t^-\rangle = -|t^-\rangle. \quad (30)$$

Based on these, we next discuss the states in the entire system. We note that P_l changes the position of the dimers in addition to the action on each dimer described above. The link parity of $|0\rangle$ is even:

$$\begin{aligned} P_l|0\rangle &= P_l (|s\rangle \cdots |s\rangle) \\ &= |\bar{s}\rangle \cdots |\bar{s}\rangle \\ &= |s\rangle \cdots |s\rangle = |0\rangle. \end{aligned} \quad (31)$$

Next we discuss the link parity of excited states in the subspace with $m = 0$. A state with a fixed position of the excited dimer is not an eigenstate of P_l nor of the momentum. For example, the state $|\text{one } t^0\rangle$ with the first dimer excited is transformed under P_l as

$$P_l (|t^0\rangle|s\rangle|s\rangle \cdots |s\rangle) = -|s\rangle|s\rangle \cdots |s\rangle|t^0\rangle.$$

On the other hand, momentum eigenstates can be constructed as a linear combination of

$$\begin{aligned} &|t^0\rangle|s\rangle|s\rangle \cdots |s\rangle, \quad |s\rangle|t^0\rangle|s\rangle \cdots |s\rangle, \\ &|s\rangle|s\rangle|t^0\rangle \cdots |s\rangle, \quad \cdots, \quad |s\rangle|s\rangle \cdots |s\rangle|t^0\rangle. \end{aligned}$$

Since the ground state $|0\rangle$ has zero momentum and \mathcal{H}_R is translationally invariant, only the zero-momentum excited states contribute to the RS spectrum. We thus only have to examine the zero-momentum combination

$$\begin{aligned} |\text{one } t^0, \tilde{q} = 0\rangle &\propto |t^0\rangle|s\rangle|s\rangle \cdots |s\rangle \\ &+ |s\rangle|t^0\rangle|s\rangle \cdots |s\rangle + \cdots \\ &+ |s\rangle|s\rangle \cdots |s\rangle|t^0\rangle. \end{aligned}$$

It turns out that this is link-parity odd:

$$P_l |\text{one } t^0, \tilde{q} = 0\rangle = -|\text{one } t^0, \tilde{q} = 0\rangle. \quad (32)$$

Since the ground state $|0\rangle$ is link-parity even, $|\text{one } t^0, \tilde{q} = 0\rangle$ appears not to have the overlap with $\mathcal{H}_R|0\rangle$. Similarly, $|\text{one } t^+, \tilde{q} = 0\rangle$ and $|\text{one } t^-, \tilde{q} = 0\rangle$ are link-parity odd, and do not have the overlap.

In the above analysis, we considered the dimerized limit $\alpha \rightarrow 0$. However, the Hamiltonian respects the link parity P_l for any α . Thus, the adiabatic continuity of the excited states, which was demonstrated numerically in Sec. IV C, implies that the corresponding states belong to the same eigenvalue of P_l for any $\alpha < \alpha_c$. It follows that, *none* of the “single elementary excitation” states $|\text{one } t^\zeta\rangle_\alpha$ ($\zeta = 0, \pm$) (corresponding to a single soliton, a single antisoliton and a single breather for $\alpha \sim \alpha_c$) contribute to the RS spectrum for $\alpha < \alpha_c$.

Thus only the states in the excitation continuum have the possibility of having non-vanishing overlap with $\mathcal{H}_R|0\rangle$. In particular, the matrix element with the “two elementary excitations” state $\langle \text{one } t^+, \text{one } t^- | \mathcal{H}_R | 0 \rangle$ does not vanish in the dimer limit. This transition is not forbidden by the selection rule due to the link parity P_l . Thus it is natural to expect that it remains non-zero for $\alpha < \alpha_c$. Indeed, we examined the matrix element $\alpha \langle \text{one } t^+, \text{one } t^- | \mathcal{H}_R | 0 \rangle_\alpha$ numerically for $\alpha < \alpha_c$. The result, obtained after extrapolation to infinite size from the systems with length 12, 14 and 16, is shown in Fig. 5. This confirms that the matrix element does not vanish within the dimer phase, as expected. The structure of excitations is continuous up to the critical point $\alpha = \alpha_c$, also in this regard.

Thus the “two elementary excitations” state $|\text{one } t^+, \text{one } t^- \rangle_\alpha$ should contribute to the RS spectrum of NENP. In the vicinity of the critical point $\alpha \sim \alpha_c$, this state may be regarded as the scattering state of a soliton and an antisoliton.

From these results, we predict that the sharp peaks corresponding to creation of single elementary excitation are absent in the RS spectrum of NTENP. The RS spectrum consists only of excitation continuum, and is qualitatively different from its INS spectrum. This difference is schematically described in Fig. 6 and Fig. 7.

VII. WEAK MAGNETIC FIELD

Finally, let us briefly discuss the effect of weak magnetic field. First we consider magnetic field H_z applied

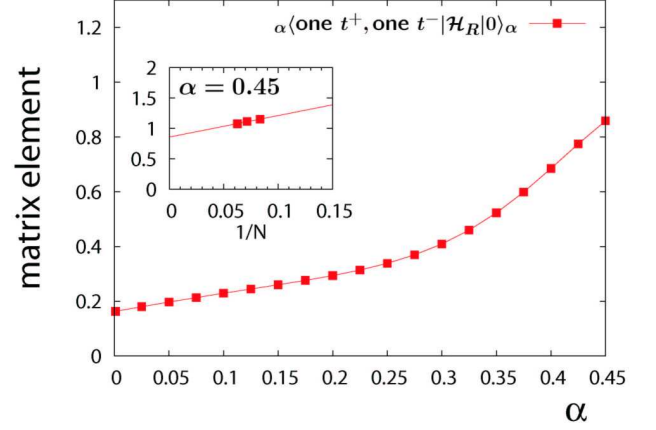


FIG. 5. The α -dependence of the matrix element $\alpha \langle \text{one } t^+, \text{one } t^- | \mathcal{H}_R | 0 \rangle_\alpha$. ($N = 16$) The state $|\text{one } t^+, \text{one } t^- \rangle_\alpha$ corresponds to the scattering state of a soliton and an antisoliton in the vicinity of the critical point $\alpha = \alpha_c$. Inset: Extrapolation of the matrix element at $\alpha = 0.45$ to $N \rightarrow \infty$.

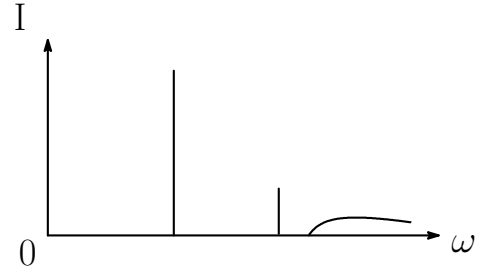


FIG. 6. Schematic view of the INS peak positions of NTENP. The first peak corresponds to the soliton and the antisoliton, and the second peak does to the breather.

in z direction. Total magnetization $\sum_j S_j^z$ is then a conserved quantity. Thus, the dispersion of each elementary excitation are simply shifted according to its magnetiza-

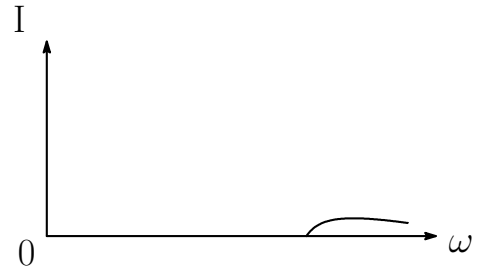


FIG. 7. Schematic view of the RS peak positions of NTENP. The sharp peaks correspond to a single elementary excitation are absent due to the selection rule.

tion as

$$\epsilon_S = \sqrt{k^2 v_s^2 + M_S^2} - H_z \quad (\text{soliton}), \quad (33)$$

$$\epsilon_{\bar{S}} = \sqrt{k^2 v_s^2 + M_S^2} + H_z \quad (\text{antisoliton}), \quad (34)$$

$$\epsilon_1 = \sqrt{k^2 v_s^2 + M_1^2} \quad (\text{1st breather}). \quad (35)$$

Phase transition occurs when the bottom of the soliton dispersion touches zero at $H_z = M_S$.

Next we consider the effect of magnetic field H_x applied perpendicular to the anisotropy axis z . In this case, the total magnetization $\sum_j S_j^z$ is no longer conserved. Therefore, a rearrangement of elementary excitations would occur. The mixing may be described by the effective 3×3 Hamiltonian in the one-soliton, one-breather, one-antisoliton subspace:

$$\mathcal{H}_{\text{eff}} = \begin{pmatrix} M_S & 0 & 0 \\ 0 & bM_S & 0 \\ 0 & 0 & M_S \end{pmatrix} - \frac{H_x}{2} \begin{pmatrix} 0 & \sqrt{2} & 0 \\ \sqrt{2} & 0 & \sqrt{2} \\ 0 & \sqrt{2} & 0 \end{pmatrix}, \quad (36)$$

where b is the mass ratio (10).

Diagonalizing this, we obtain the masses of 3 elementary excitations in the transverse magnetic field as

$$M_A = M_S, \quad (37)$$

$$M_{\pm} = \frac{(1+b)M_S \pm \sqrt{M_S^2(b-1)^2 + 4H_x^2}}{2}. \quad (38)$$

Namely, one of the elementary excitations (which is an antisymmetric linear combination of soliton and antisoliton) has constant mass M_S . The other two masses depend nonlinearly on H_x . The lowest mass M_- is reduced to zero at a critical field, where a phase transition occurs.

This is essentially identical to the preceding analysis of anisotropic Haldane chains in Ref. 28 which was applied to NDMAP²⁹ and NTENP^{15,25}, where the in-plane anisotropy E is also taken into account. As pointed out in Refs. 15 and 17, the scattering intensity corresponding to the higher-energy elementary excitation (with the M_+) is suppressed in a moderate transverse field, where the elementary excitation is absorbed into the excitation continuum. Systematic analysis of the effects of the transverse field in the SG theory framework is left for future. This will be necessary for discussion of ESR spectra²⁵ in the present approach.

VIII. SUMMARY AND DISCUSSION

In this study, we found that the low-energy excitations of NTENP are well described in the framework of the SG field theory. The elementary excitations of NTENP correspond to the soliton, the antisoliton and the breather, which are respectively created by applying S_q^+ , S_q^- and S_q^z on the ground state. Their correspondence

with the original spin model is deduced from the dimer limit $\alpha = 0$, where the original model is exactly solvable, and the numerical exact diagonalization calculation which shows that the excitation structure is smoothly connected from the dimer limit $\alpha = 0$ to $\alpha \sim \alpha_c$. This picture of excitations well explains the preceding INS experiments on NTENP and numerical calculations of the DSF.

Based on the established picture, we found that the sharp peaks, each of which corresponds to a single elementary excitation, vanish in the RS spectrum of NTENP. This is qualitatively distinct from the INS spectrum. A slight disagreement with the experiments may be caused by the neglect of the E term anisotropy in the model Hamiltonian (2), and the use of the effective field theory, which is only asymptotically exact in the low-energy limit,

Although our primary focus in this paper was NTENP, the present result could be applied to other systems in the dimer phase of the Hamiltonian (2). Depending on the value of the uniaxial anisotropy D , the number of breathers changes: The system has two breathers for $0 \leq D \lesssim 0.1J$, one breather for $0.1J \lesssim D \lesssim 0.5J$ and no breather for $0.5J \lesssim D$.

Besides the bond-alternating chain (2), there are also completely different class of systems that are described by the SG field theory. An example in quantum magnetism is the $S = 1/2$ antiferromagnetic chain with a staggered field. It describes several materials in a magnetic field, such as Cu benzoate. While this system is physically quite different from the model discussed in the present paper, they are both described by SG theory.³⁰ The difference appears in the correspondence between the spin operators and the boson field. In fact, in the staggered field case, soliton and antisoliton couple to S^z while n -th breather couples to S^x if n is even, and to S^y if n is odd. (Here we define the direction of the staggered field as x direction.) As a consequence, observable spectra are quite different from the $S=1$ chain studied in the present paper.

As a final remark, in the context of the SG field theory, difference between the dimer phase and the Haldane phase is nothing but the sign of the cosine term in the Lagrangian density (6). This change should not yield a qualitative difference in the properties of the SG theory, although its physical consequences may be altered. The SG field theory could provide a starting point for a unified understanding of dynamics in different phases of $S = 1$ antiferromagnetic chains. In a related but somewhat different context, anisotropic $S = 1$ chains without bond alternation was studied in terms of SG theory.³¹ It would be interesting to compare the two systems in more detail.

ACKNOWLEDGMENT

The authors thank, in particular, Shunsuke C. Furuya, Sei-ichiro Suga, and Takafumi Suzuki for valuable discussions which were essential to complete the present work. The authors are also grateful to Masayuki Hagiwara, Yuhei Natsume, Hidetoshi Nishimori, Kiyomi Okamoto,

and Shintaro Takayoshi for useful comments. The numerical calculations in this paper are based on KOBEPACK version 1.0 by Takashi Tonegawa, Makoto Kaburagi and Tomotoshi Nishino. This work is supported in part by a Grant-in-Aid for scientific research (KAKENHI) Nos. 21540381 and 20102008, and by the 21st Century COE program at Tokyo Institute of Technology “Nanometer-Scale Quantum Physics”, both from MEXT of Japan.

-
- * Corresponding author
- ¹ F. D. M. Haldane, Phys. Lett. A **93**, 464 (1983); Phys. Rev. Lett. **50**, 1153 (1983).
 - ² I. Affleck, J. Phys.: Condens. Matter **1**, 3047 (1989).
 - ³ I. Affleck, T. Kennedy, E. H. Lieb, and H. Tasaki, Phys. Rev. Lett. **59**, 799 (1987).
 - ⁴ I. Affleck, Nucl. Phys. B **257** [FS14], 397 (1985); Nucl. Phys. B **265** [FS15], 409 (1986).
 - ⁵ I. Affleck and F. D. M. Haldane, Phys. Rev. B **36**, 5291 (1987).
 - ⁶ T. Kennedy and H. Tasaki, Phys. Rev. B **45**, 304 (1992).
 - ⁷ M. Oshikawa, J. Phys.: Condens. Matter **4**, 7469 (1992).
 - ⁸ M. den Nijs and K. Rommelse, Phys. Rev. B **40**, 4709 (1989).
 - ⁹ F. Pollmann, E. Berg, A. M. Turner, and M. Oshikawa, Phys. Rev. B **85**, 075125 (2012).
 - ¹⁰ F. Pollmann, A. M. Turner, E. Berg, and M. Oshikawa, Phys. Rev. B **81**, 064439 (2010).
 - ¹¹ A. Escuer, R. Vicente and X. Solans, J. Chem. Soc. Dalton Trans. **(1997)**, 531.
 - ¹² M. Hagiwara, Y. Narumi, K. Kindo, M. Kohno, H. Nakano, R. Sato, and M. Takahashi, Phys. Rev. Lett. **80**, 1312 (1998).
 - ¹³ Y. Narumi, M. Hagiwara, M. Kohno, and K. Kindo, Phys. Rev. Lett. **86**, 324 (2001).
 - ¹⁴ A. Zheludev, T. Masuda, B. Sales, D. Mandrus, T. Papenbrock, T. Barnes, and S. Park, Phys. Rev. B **69**, 144417 (2004).
 - ¹⁵ M. Hagiwara, L. P. Regnault, A. Zheludev, A. Stunault, N. Metoki, T. Suzuki, S. Suga, K. Kakurai, Y. Koike, P. Vorderwisch, and J. H. Chung, Phys. Rev. Lett. **94**, 177202 (2005).
 - ¹⁶ L. P. Regnault, M. Hagiwara, N. Metoki, Y. Koike, K. Kakurai, and A. Stunault, Physica B **350**, 66 (2004).
 - ¹⁷ T. Suzuki and S.-i. Suga, Phys. Rev. B **72**, 014434 (2005).
 - ¹⁸ W. Chen, K. Hida, and B. C. Sanctuary, J. Phys. Soc. Jpn. **69**, 237 (2000); *ibid.* **77**, 118001(E) (2008).
 - ¹⁹ See, for example, D. Sénéchal, in *Theoretical Methods for Strongly Correlated Electrons*, edited by D. Sénéchal, A.-M. Tremblay, and C. Bourbonnais (Springer, Berlin, 2003), [arXiv:cond-mat/9908262](#); A. O. Gogolin, A. A. Nersisyan and A. M. Tsvelik, *Bosonization and Strongly Correlated Systems*, (Cambridge University Press, Cambridge, 2004).
 - ²⁰ H. Bergknoff and H. B. Thacker, Phys. Rev. D **19**, 3666 (1979).
 - ²¹ V. E. Korepin, Theor. Math. Phys. **41**, 169 (1979).
 - ²² G. Bouzerar, A. P. Kampf, and G. I. Japaridze, Phys. Rev. B **58**, 3117 (1998).
 - ²³ S. Takayoshi and M. Oshikawa, [arXiv:1201.2030](#).
 - ²⁴ H. J. Schulz, Phys. Rev. B **34**, 6372 (1986).
 - ²⁵ V. N. Glazkov, A. I. Smirnov, A. Zheludev, and B. C. Sales, Phys. Rev. B **82**, 184406 (2010).
 - ²⁶ J. B. Parkinson, J. Phys. C **2**, 2012 (1969); S. Bacci and E. Gagliano, Phys. Rev. B **43**, 6224 (1991).
 - ²⁷ M. Sato, H. Katsura, and N. Nagaosa, [arXiv:1105.2259](#).
 - ²⁸ O. Golinelli, Th. Jolicœur, and R. Lacaze, J. Phys.: Condens. Matter **5**, 7847 (1993).
 - ²⁹ A. Zheludev, Y. Chen, C. L. Broholm, Z. Honda, and K. Katsumata, Phys. Rev. B **63**, 104410 (2001).
 - ³⁰ M. Oshikawa and I. Affleck, Phys. Rev. Lett. **79**, 2883 (1997); I. Affleck and M. Oshikawa, Phys. Rev. B **60**, 1038 (1999); Phys. Rev. B **62**, 9200(E) (2000).
 - ³¹ L. Campos Venuti, C. Degli Esposti Boschi, E. Ercolessi, G. Morandi, F. Ortolani, S. Pasini and M. Roncaglia, Eur. Phys. J. B **53**, 11 (2006).